Designing redder and brighter fluorophores by synergistic tuning of ground and excited states

SCHOLARONE™
Manuscripts

Journal Name

COMMUNICATION

Designing redder and brighter fluorophores by synergistic tuning of ground and excited states

Cheng Chen,[a] Mikhail S. Baranov,[bc] Liangdong Zhu,[a] Nadezhda S. Baleeva,[b] Alexander Yu. Smirnov,[b] Snizhana O. Zaitseva,[b] Ilia V. Yampolsky,[bc] Kyril M. Solntsev,[de] and Chong Fang*[a]
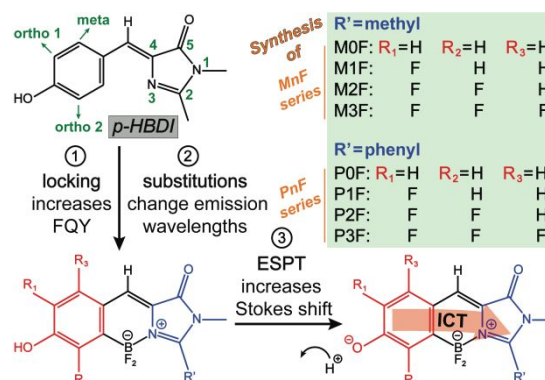
We strategically modified the GFP core via chemical synthesis to make redder and brighter biomimetic fluorophores. Based on quantum calculations, solvatochromism analysis, and femtosecond Raman, we unveiled the additive effect of tuning the electronic ground and excited states, respectively, to achieve a dramatic emission redshift with a "double-donor-one-acceptor" structure.

Organic fluorophores have increasingly drawn interest for bioimaging due to their engineerable sensitivity and selectivity, ease of synthesis, and low cost, etc.[1] Ideal fluorescent probes require red emission to improve penetration depths and avoid tissue autofluorescence, with high fluorescence quantum yield (FQY) and large Stokes shifts to increase the imaging signal-to-noise ratio (SNR). Although emission redshift in systems such as heteroatom rhodamine[2] and cyanine derivatives[3] was shown, current development of fluorescent probes remains largely trial and error, lacking efficiency or insights. Synthetic fluorophores also suffer from certain drawbacks. For instance, an extended π-conjugation is commonly used, but the lack of fundamental understanding could lead to an inefficient use of structure.[3-4] The large molecular size may limit its applications such as neural imaging due to the blood-brain barrier.[5] Meanwhile, the long-chain design promotes nonradiative pathways via twisting or isomerization, reducing the FQY.[6] In addition, the most widely used fluorescent dyes like cyanine and rhodamine have small

Stokes shifts, causing poor SNR in imaging.[7] Therefore, deeper mechanistic insights are crucial for the rational design of redder and brighter fluorescent probes with a large Stokes shift.

Herein, we present an effective red-shifting strategy from an integrated spectroscopic and computational characterization of two series of fluorophores, MnF and PnF, derived from the GFP model chromophore p-HBDI (Scheme 1; see chemical synthesis methods in ESI†) with a benzylidene imidazolones (BDIs) core.[8] As biomimetics, the locked p-HBDI derivatives were synthesized by a coordination-assisted borylation reaction that is effective in synthesizing various fixed BDIs' analogs.[8b,9] These compounds are brightly colored and highly soluble in water and other polar solvents, making them versatile fluorescent or fluorogenic sensors. Similar BF_2 coupling strategy has also been applied and achieved successes in other molecular systems such as BODIPY-based dyes.[10] Moreover, several BDIs demonstrate a high degree of photoinduced intramolecular charge transfer (ICT), leading to an additional excited state in aminated derivatives[9a] or high photoacidity in hydroxylated BDIs.[8b,11] In this work, strategic substitutions at phenolate (donor) and imidazolinone (acceptor) rings enable a separate tuning of HOMO and LUMO energy, in an additive manner, to redshift emission of the locked GFP core in solution. This principle can help develop red/near-

a. *Department of Chemistry, Oregon State University, 153 Gilbert Hall, Corvallis, OR 97331, USA. *E-mail: Chong.Fang@oregonstate.edu (C.F.); Fax: +1 541 737 2062; Tel: +1 541 737 6704; Web: https://fanglab.oregonstate.edu/.*

b. *Institute of Bioorganic Chemistry, Russian Academy of Sciences, Miklukho-Maklaya 16/10, Moscow 117997, Russia.*

c. *Pirogov Russian National Research Medical University, Ostrovitianov 1, Moscow 117997, Russia.*

d. *School of Chemistry and Biochemistry, Georgia Institute of Technology, Atlanta, Georgia 30332, USA.*

e. *New York University Abu Dhabi, P.O. Box 129188, Abu Dhabi, UAE.*

† Electronic Supplementary Information (ESI) available: Detailed synthesis methods of all the new compounds, calculated frontier molecular orbitals and HOMO-LUMO energy gaps, UV-Visible and fluorescence spectra, the FQY data, solvatochromism analysis, Fig. S1–S7, Table S1–S8, and the ^1H, ^{13}C, and ^{19}F NMR spectra of the newly synthesized compounds as an Appendix (Fig. S8–S71). See DOI: 10.1039/x0xx00000x

Scheme 1 Design routes for GFP-chromophore derivatives with redder emission, higher fluorescence quantum yield, and larger Stokes shift

IR fluorophores without significant extension of π-conjugation. Besides, excited-state proton transfer (ESPT) results in large Stokes shifts up to 150 nm between the neutral form absorption and anionic form emission. Conformational locking and addition of a sidechain phenyl group can also benchmark effects of the backbone and sidechain flexibility on FQY, corroborated in part by previous studies on the aggregation-induced emission and a series of modified fluorescent molecular rotors.[12]

We first examined the photophysical properties of MnF and PnF (see Table 1). Cumulative fluorination leads to an emission redshift from 0F→2F but a blueshift from 2F→3F in both series. We performed the time-dependent density functional theory (TD-DFT) calculations at the RB3LYP/6-311G(d,p) level[13] and unveiled the correlations between the radiative emission and electronic structures. Since TD-DFT optimization produces a relaxed excited-state geometry, the HOMO-LUMO energy gap could be used to estimate the emission peak wavelength.[14]

The emission turning point upon cumulative fluorination is reproduced by our calculations. Fig. 1a and b show the electron density distribution of HOMO and LUMO for the locked HBDI scaffolds with no fluorination (M0F, P0F). The largest oscillator strength indicates that HOMO→LUMO transition is primarily $S_0 \to S_1$. Notably, two *ortho* sites to the phenolic hydroxyl are electron rich whereas the *meta* site is deficient in HOMO. This is because the phenolate–$O^{(-)}$ is a strong electron-donating group (EDG), thereby increasing and decreasing the electron density at its *ortho* and *meta* sites, respectively, on a "push-pull" π-conjugated system.[6] The LUMO, however, shows similar electron densities at these sites after charge redistribution. Since electrophilic substitutions at nucleophilic sites lower the HOMO and LUMO energies (Fig. 1c),[4,15] the emission redshift from 0F to 2F arises from better stabilization of LUMO than HOMO by fluorination. The *meta*-site fluorination seems to grant more stability to HOMO than LUMO despite its electron deficiency in S_0, leading to a blue-shifted emission in 3F.

To gain more insights into the color tuning, we simulated substitutions at the phenolate ring by –CN and –NH_2 in single- and multi-site fashions (Fig. 1, 2 and S1, ESI†). As predicted, the electron-withdrawing group (EWG) –CN at *ortho* sites stabilizes HOMO whereas the EDG –NH_2 strongly destabilizes HOMO due to antibonding interactions (see the node between nitrogen

and the ring, Fig. S2 and S4, ESI†). Interestingly, EWG at the *meta* site stabilizes HOMO while EDG has a marginal effect (Fig. 2).

Notably, the stabilization/destabilization effect on LUMO by the EWG/EDG at nucleophilic sites is weaker than that on HOMO except for fluorine. This is because: (1) LUMO is more delocalized and corresponds to a larger "quantum box" than HOMO, thus bearing smaller impact by substitutions; (2) the excited-state ICT reduces electron density on the phenolate ring. As a result, substituents at the donor moiety have less orbital contributions to LUMO, confirmed by a decreased electron density on the substituents from HOMO to LUMO (see Fig. S2–S5, ESI†), with a more dramatic effect for EDGs. This investigation underpins a key strategy of incorporating EDG at the donor site(s) to destabilize HOMO with minor change on LUMO. Moreover, EWGs (–F and –CN) exhibit an additive effect on HOMO energy from mono- to tri-substitution whereas such effect is insignificant for EDGs (–NH_2) due to a restructured orbital by amination next to another donor (Fig. 1c, S1, S2 and S4, ESI†). This "double-donor" structure (i.e., a phenolate $O^{(-)}$ and an adjacent EDG, see Scheme 2) may constitute an effective configuration to promote redder emission, which, to the best of our knowledge, has been underexplored. However, as a word of caution, large conjugated EDGs are not recommended because the extra stability may cancel the destabilization effect for HOMO (Table S5, ESI†). Halogens show an opposite effect that LUMO is stabilized more than HOMO due to the competing electron-donating resonance (+Re) and electron-withdrawing inductive (–I) effects that may partially cancel each other.[15]
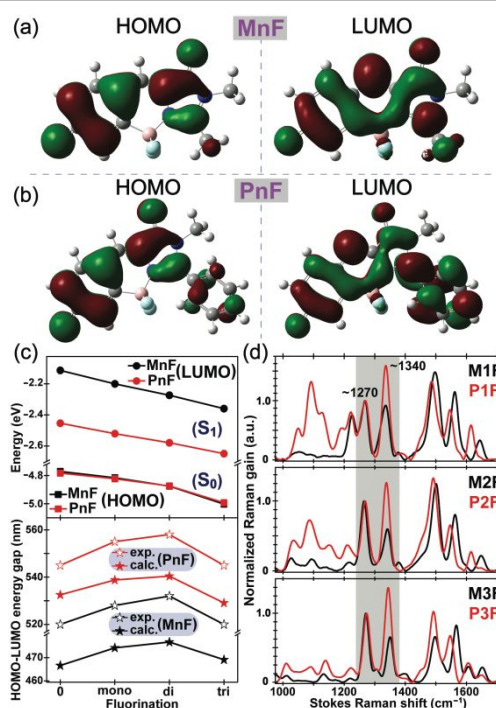

Fig. 1 HOMO /LUMO electron density distributions of M0F (a) and P0F (b) from TD-DFT calculations of the anionic chromophore. (c) Calculated HOMO/LUMO energies and gaps of MnF and PnF (n=0–3) with cumulative fluorination. Experimental anionic form emission wavelengths are shown. (d) Ground state FSRS for MnF and PnF (n=1–3) with the picosecond Raman pump at 560 nm.

Table 1 Photophysical properties of MnF and PnF in water

Compd.	neutral		anionic		$\Phi_F{}^b$	$\Phi'_F{}^c$	$\Phi_{PT}{}^d$
	$\lambda_{abs}{}^a$	$\lambda_{em}{}^a$	$\lambda_{abs}{}^a$	$\lambda_{em}{}^a$			
M0F	404	485	485	520	0.28	0.77	0.36
M1F	401	n.d.[e]	485	528	0.41	0.64	0.64
M2F	394	n.d.[e]	479	532	0.51	0.66	0.77
M3F	393	n.d.[e]	474	520	0.55	0.66	0.83
P0F	422	503	512	545	0.12	0.34	0.35
P1F	416	n.d.[e]	511	555	0.25	0.36	0.69
P2F	409	n.d.[e]	508	558	0.27	0.38	0.71
P3F	406	n.d.[e]	499	545	0.33	0.45	0.73

[a] Peak maximum in nm. [b] Anionic FQY upon excitation of the neutral form. [c] Anionic FQY upon excitation of the anionic form. [d] ESPT quantum yield, calculated as the ratio of Φ_F/Φ'_F. [e] Not detected due to the highly efficient ESPT in water.

Notably, the HOMOs of MnF and PnF with same fluorination remain isoenergetic, independent of substitution sites (Fig. 1c and 2). This also applies to −CN and −NH$_2$ substitutions (Fig. 2, S2 and S4, ESI†). Redder emission of PnF arises from its lower LUMO energy due to a larger "box" size enabled by ICT. In essence, the extended electron π-conjugation by phenyl mainly results in the stabilization of LUMO instead of a simultaneous stabilization of both HOMO and LUMO as commonly assumed.

To provide further experimental support, we performed the tunable femtosecond stimulated Raman spectroscopy (FSRS)[16] to retrieve vibrational signatures that are sensitive to local structure.[17] The ~1270 and 1340 cm^{-1} marker bands involve motions across the locked rings and are good indicators for local electron density (Table S1, ESI†). Ground-state FSRS shows that MnF and PnF have nearly identical frequencies for these modes (Fig. 1d), so replacement of methyl by phenyl does not induce noticeable charge transfer and S$_0$ stabilization. Remarkably, the time-resolved excited-state FSRS spectra exhibit clear mode frequency shifts and infers a transient ICT. In particular, the ~1340 cm^{-1} imidazolinone C−N stretching and bridge-H rocking motion blueshifts by 23 or 13 cm^{-1} from S$_0$→S$_1$ of the anionic M3F or P3F in water (Fig. S6, ESI†).[11] This key result confirms that electron density on the imidazolinone ring increases in the excited state due to ICT. In addition, negative solvatochromism is found in the emission spectra using fourteen solvents from water to pyridine: ca. 20–30 nm shift for MnF, 45–60 nm shift for PnF (Tables S2 and S3, ESI†).[18] Kamlet-Taft analysis[8b] reveals a negative correlation between the spectral shift and solvent
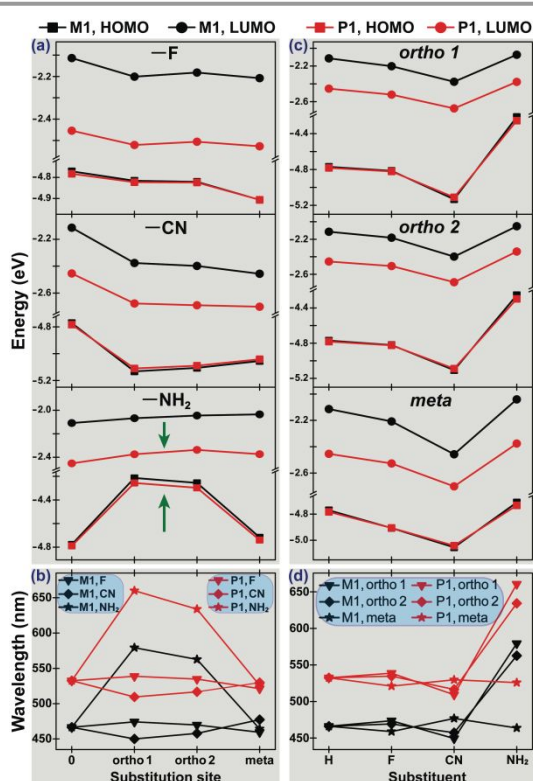

Fig. 2 Substitution effects at various conditions by quantum calculations. Calculated HOMO/LUMO energies (a) and gaps (b) of single-site substitutions at different sites. Calculated HOMO/LUMO energies (c) and gaps (d) of single-site substitutions by different substituents. Green arrows denote synergistic tuning.

Scheme 2 "Double-donor-one-acceptor" and systematic tuning with the EDGs and EWG at opposite ends of the chromophore for redder emission
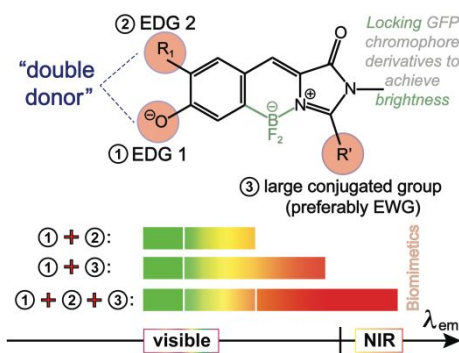
polarity (Table S4, ESI†),[8b] which indicates a decreased dipole moment in S$_1$ and further verifies the ICT process (Scheme 1).

These crucial insights enable another red-shifting strategy: introducing large π-conjugated groups to the 2-position of the imidazolinone ring to increase "box" size and lower the excited state energy with the ground state largely unaffected. Though strong EWGs at the imidazolinone end pull electrons and provide stability for HOMO, it is overwhelmed by the energy lowering of LUMO. In aggregate, we propose a unique "double-donor-one-acceptor" approach to achieve red-shifted emission through a synergistic tuning of the ground and excited state energies by applying small EDGs and EWGs at the phenolate and imidazolinone ends, respectively (see Scheme 2). Simulations of various substituents (Table S5, ESI†) imply that this strategy could lead to near-IR emission while keeping a small molecular size (e.g., to diminish nonradiative decay pathways of S$_1$).[17b,19]

To corroborate this tuning strategy, while limited by current borylation process to incorporate functional groups (ESI† text), we synthesized various unlocked HBDIs (Fig. 3). The "additive" effect manifests: the fluorophore emission redshifts with the increasing ED ability of R$_1$ substituent (cyano-, methoxy-, hydroxy-, amino-, etc.) and conjugation size or EW ability of R' substituent (methyl, phenyl, styryl, vinylpyridine), validating the generality of this "double-donor-one-acceptor" design concept. Moreover, the ring coplanarity should further redshift the emission,[11,20] substantiated by a notable redshift (ca. 500→520 nm) from the *p*-HBDI anionic chromophore[11,21] to the locked version (i.e., M0F). The measured FQYs of unlocked compounds are <2×10^{-3} (Table S8). We expect future locking methods to fully achieve their red-shifting potential and improve FQY.[9b,12b]

Furthermore, high brightness with redder emission remains a marked challenge due to the interplay between radiative and nonradiative decay pathways. Here, the conformational locking by a BF$_2$ group inhibits the twisting-induced internal conversion and enhances FQY by several orders of magnitude from ~10^{-4} in *p*-HBDI[8,11] to >10^{-1} in MnF. The incorporation of a sidechain phenyl leads to a FQY drop by ~2 folds (Table 1) compared to MnF due to phenyl ring twisting. These results suggest that the backbone flexibility has a much higher impact on FQY than the sidechain flexibility. Also, with ESPT the anionic form FQY upon neutral excitation (Φ_F) is lower than direct anionic excitation (Φ'_F). They are linearly correlated with the ESPT efficiency (Φ_{PT}) that depends on the photoacidity of the chromophore (Table 1):
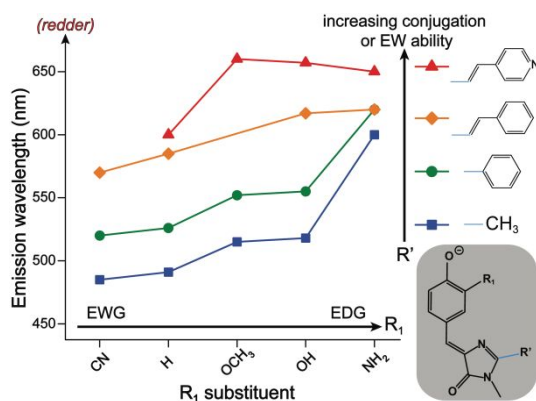
Fig. 3 Substituent effects of the R_1 and R' sites on emission wavelength of the anionic form in water based on the unlocked *p*-HBDI backbone. Two compounds with R_1=CN (red) and OCH_3 (orange) are absent due to the unavailability of synthesis and abnormal spectral behavior, respectively. See Table S7 (ESI†) for the electronic absorption and emission properties.

$$\Phi_F = \frac{k_{PT}}{k_{nr} + k_F + k_{PT} + k'_{PT}} \cdot \frac{k'_F}{k'_{nr} + k'_F} = \Phi_{PT} \cdot \Phi'_F$$

where k_F (k'_F), k_{nr} (k'_{nr}) represent the rate constants of fluorescence, nonradiative decays of the neutral (anionic) form, respectively. k_{PT} and k'_{PT} is the adiabatic and diabatic ESPT rate constant, respectively.[8b,22] The excited-state pK_a^* values (Table S6, ESI†) show that photoacidity increases from 0F→3F for both series, consistent with their increasing Φ_{PT} and FQYs (Φ_F).

Regarding the Stokes shift, ESPT is effective because it involves a downhill reaction from a protonated to deprotonated state. Considering an intrinsic difference between absorption and emission of the same species (by vibrational relaxation), the Stoke shift after ESPT is more dramatic. In fact, an enhanced ICT character should improve the Stokes shift due to a more stable electronic structure than the locally excited state.[9a,11,19] Previous efforts to enlarge Stokes shift such as constructing an asymmetric structure[23] or donor-acceptor system[6] essentially modified the ICT properties in a push-pull π-conjugated system.

In conclusion, we have devised a unique red-shifting strategy by synthesizing two new series of GFP chromophore derivatives in aqueous solution, aided by quantum calculations of frontier molecular orbitals, electronic and vibrational spectroscopies in S_0 and S_1, and systematic synthesis of the substituted (at both the donor and acceptor sites) unlocked HBDIs. We reveal that the electronic ground and excited states can be tuned by a range of EDGs and conjugated groups/EWGs at the phenolate and imidazolinone ends, respectively, with an additive effect to achieve redder emission. In conjunction with ESPT capabilities enabled by photoacidity and further conformational locking of the backbone, these foundational design routes for redder and brighter fluorophores in solution will inspire chemical synthesis methods and advance a broad range of imaging applications.

Conflicts of interest

There are no conflicts to declare.

Notes and references

1   (*a*) M. S. T. Goncalves, *Chem. Rev.*, 2009, **109**, 190-212; (*b*) L. Yuan, W. Lin, K. Zheng, L. He and W. Huang, *Chem. Soc. Rev.*, 2013, **42**, 622-661.
2   X. Chai, X. Cui, B. Wang, F. Yang, Y. Cai, Q. Wu and T. Wang, *Chem. Eur. J.*, 2015, **21**, 16754-16758.
3   G. M. Fischer, E. Daltrozzo and A. Zumbusch, *Angew. Chem. Int. Ed.*, 2011, **50**, 1406-1409.
4   E. Kim, M. Koh, B. J. Lim and S. B. Park, *J. Am. Chem. Soc.*, 2011, **133**, 6642-6649.
5   O. Veiseh, C. Sun, C. Fang, N. Bhattarai, J. Gunn, F. Kievit, K. Du, B. Pullar, D. Lee, R. G. Ellenbogen, et al., *Cancer Res.*, 2009, **69**, 6200-6207.
6   N. Karton-Lifshin, L. Albertazzi, M. Bendikov, P. S. Baran and D. Shabat, *J. Am. Chem. Soc.*, 2012, **134**, 20412-20420.
7   (*a*) Z. Zhang and S. Achilefu, *Org. Lett.*, 2004, **6**, 2067-2070; (*b*) C. Liu, X. Jiao, Q. Wang, K. Huang, S. He, L. Zhao and X. Zeng, *Chem. Commun.*, 2017, **53**, 10727-10730.
8   (*a*) A. F. Bell, X. He, R. M. Wachter and P. J. Tonge, *Biochemistry*, 2000, **39**, 4423-4431; (*b*) M. S. Baranov, K. A. Lukyanov, A. O. Borissova, J. Shamir, D. Kosenkov, L. V. Slipchenko, L. M. Tolbert, I. V. Yampolsky and K. M. Solntsev, *J. Am. Chem. Soc.*, 2012, **134**, 6025-6032.
9   (*a*) M. S. Baranov, K. M. Solntsev, N. S. Baleeva, A. S. Mishin, S. A. Lukyanov, K. A. Lukyanov and I. V. Yampolsky, *Chem. Eur. J.*, 2014, **20**, 13234-13241; (*b*) N. S. Baleeva, K. A. Myannik, I. V. Yampolsky and M. S. Baranov, *Eur. J. Org. Chem.*, 2015, **2015**, 5716-5721.
10 G. Ulrich, R. Ziessel and A. Harriman, *Angew. Chem. Int. Ed.*, 2008, **47**, 1184-1201.
11 C. Chen, W. Liu, M. S. Baranov, N. S. Baleeva, I. V. Yampolsky, L. Zhu, Y. Wang, A. Shamir, K. M. Solntsev and C. Fang, *J. Phys. Chem. Lett.*, 2017, **8**, 5921-5928.
12 (*a*) Y. Hong, J. W. Y. Lam and B. Z. Tang, *Chem. Soc. Rev.*, 2011, **40**, 5361-5388; (*b*) H. Qian, M. E. Cousins, E. H. Horak, A. Wakefield, M. D. Liptak and I. Aprahamian, *Nat. Chem.*, 2017, **9**, 83-87.
13 (*a*) O. V. Gritsenko, P. R. T. Schipper and E. J. Baerends, *J. Chem. Phys.*, 1997, **107**, 5007-5015; (*b*) M. J. Frisch, et al., *Gaussian 09*, Revision B.1, Gaussian, Inc., 2009.
14 C. Adamo and D. Jacquemin, *Chem. Soc. Rev.*, 2013, **42**, 845-856.
15 N. Hashimoto, R. Umano, Y. Ochi, K. Shimahara, J. Nakamura, S. Mori, H. Ohta, Y. Watanabe and M. Hayashi, *J. Am. Chem. Soc.*, 2018, **140**, 2046-2049.
16 W. Liu, Y. Wang, L. Tang, B. G. Oscar, L. Zhu and C. Fang, *Chem. Sci.*, 2016, **7**, 5484-5494.
17 (*a*) C. Fang, R. R. Frontiera, R. Tran and R. A. Mathies, *Nature*, 2009, **462**, 200-204; (*b*) C. Fang, L. Tang, B. G. Oscar and C. Chen, *J. Phys. Chem. Lett.*, 2018, **9**, 3253–3263.
18 X. Peng, F. Song, E. Lu, Y. Wang, W. Zhou, J. Fan and Y. Gao, *J. Am. Chem. Soc.*, 2005, **127**, 4170-4171.
19 N. Amdursky, Y. Erez and D. Huppert, *Acc. Chem. Res.*, 2012, **45**, 1548-1557.
20 Z. Piontkowski and D. W. McCamant, *J. Am. Chem. Soc.*, 2018, **140**, 11046-11057.
21 N. M. Webber, K. L. Litvinenko and S. R. Meech, *J. Phys. Chem. B*, 2001, **105**, 8036-8039.
22 A. L. Sobolewski and W. Domcke, *J. Phys. Chem. A*, 2007, **111**, 11725-11735.
23 T.-B. Ren, W. Xu, W. Zhang, X.-X. Zhang, Z.-Y. Wang, Z. Xiang, L. Yuan and X.-B. Zhang, *J. Am. Chem. Soc.*, 2018, **140**, 7716-7722.